A slope-theory approach to electrical probe recording on phase-change media

Mustafa M. Aziz[a] and C. David Wright
School of Engineering, Computer Science and Mathematics, University of Exeter, Harrison Building, Exeter EX4 4QF, United Kingdom

(Received 28 October 2004; accepted 14 March 2005; published online 16 May 2005)

A theoretical approach to predicting the spatial extent of the amorphous to crystalline transition region during the probe recording process on phase-change storage media is presented. The extent of this transition region determines the ultimate achievable linear density for data storage using phase-change materials. The approach has parallels with the slope theory used to find magnetic transition lengths in magnetic recording, and shows that the amorphous to crystalline transition length can be minimized by reducing the thickness of the phase-change layer, by minimizing lateral heat flow, and by maximizing the ratio of the activation energy for crystallization to the transition temperature E_c/T_t. © *2005 American Institute of Physics*. [DOI: 10.1063/1.1904156]

I. INTRODUCTION

In striving towards the achievement of higher areal storage densities, storage technologies that involve microscopic probes are emerging. These probes are used to induce semipermanent, nanoscale changes in storage media to record the binary data. One approach involved using highly conductive tips, either in contact (using modified atomic force microscope tips)[1–3] or in close proximity (using scanning tunneling microscope tips)[1,4,5] to a phase-change medium to deliver a current that, through Joule heating, induces stable amorphous or crystalline phase transformations to record information. Using these techniques, it was shown that it is possible to record stable crystalline marks in an amorphous material with diameters less than 50 nm.[3,5] The amorphous regions are characterized by low electrical conductivity, while the crystalline or semimetal regions are characterized by high electrical conductivity. Hence Ohm's law can be relied upon in detecting this difference in conductivity as changes in the sense current of the scanning tip when a constant potential is applied between the tip and the recording layer.

Figure 1 shows a typical characteristic curve illustrating the change in conductivity of an amorphous phase-change film with temperature,[6] where the arrows indicate the heating and cooling cycles. This figure shows that conductivity of the amorphous material increases gradually with temperature, and switches irreversibly to a high conducting crystalline state beyond a characteristic temperature T_t, which will be referred to here as the transition temperature. Cooling to room temperature followed by heating beyond this transition temperature, the material will maintain its high conducting crystalline state with conductivity that is almost four orders of magnitude greater than that of the amorphous phase. This memory feature and the large difference in the electrical conductivity of the two states make phase-change media attractive for scanning probe and solid-state storage devices. Heating to temperatures below the transition temperature followed by cooling will cause the material to revert back to the original low-conductivity amorphous state.

The recording process in electrical probe storage is complex and involves transient electrical and thermal processes to induce the phase transformation. The kinetics of the crystallization and amorphization processes of the phase-change layer also play an important role in determining the stability and size of the recorded marks. Recently, a finite element computational model was used to successfully simulate the record, readout, and erase processes in a phase-change structure in physical contact with a microscopic conductive tip.[7,8] This dynamic electrothermal numerical model was used to optimize the thermal and electrical properties of the structure to achieve the required temperature distributions in the recording layer. Through inclusion of classical models for crystallization, moreover, this model was able to predict the shape and size of the recorded marks throughout the depth of the phase-change layer. These were later used to predict the readout signals. With the wealth of information they provide and their detail, it is, however, difficult with numerical models to examine quickly and simply the relationships and dependencies between the different parameters of the storage system as a whole, and to study their influence on recording

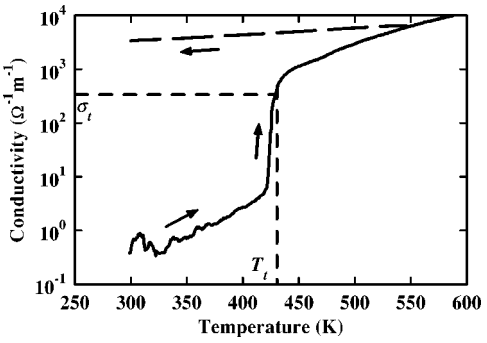

FIG. 1. Four-point-probe measurement of conductivity vs temperature of an 80-nm $Ge_2Sb_2Te_5$ film heated at a rate of 1.6 K/min (see Ref. 6). The dashed line is for heating up to 270 °C at 1.2 K/min and cooling to room temperature. The transition temperature T_t at 1.6 K/min is estimated to be 430 K from the maximum of the slope of conductivity vs temperature.

[a]Electronic mail: m.m.aziz@ex.ac.uk

performance. Analytical models, although approximate, are more attractive in this sense and offer expressions that can display these dependencies clearly and explicitly.

The aim of this work therefore is to provide a theoretical treatment of the process of recording a crystalline mark in an amorphous material, using an electrically conductive tip in contact with a phase-change material, that combines the electrothermal and kinetic processes involved using an analytical slope-theory technique. This will be used to predict the extent of the amorphous to crystalline transition along the recording layer. The spatial extent of this transformation boundary limits how closely marks can be written next to each other, and hence determines the possible linear density of the storage system.

Slope theory has its origins in magnetic recording[9,10] as a way of modeling the complex magnetic recording process, including the influences of the head-to-medium geometry and interface parameters and the bulk properties of the storage medium, in a self-consistent approach. This theory has been proven successful in underlining the factors that limit the spacing between magnetic bits and has been used by many researches to provide directions on how to increase the storage densities in hard disk drives and other magnetic storage systems.[11]

The premise of the slope theory lies in the determination of the spatial gradient of the transition region between adjacent "bits" (amorphous and crystalline regions in phase-change storage media; positively and negatively magnetized regions in magnetic storage media) in the storage layer. The gradient is obtained by the solution of the slope equation which, for the case of electrical writing into phase-change media, can be written as

$$\frac{\partial \sigma_p}{\partial x} = \frac{\partial \sigma_p}{\partial T}\frac{\partial T}{\partial x}, \tag{1}$$

where σ_p is the conductivity profile along the x direction, and T is the temperature in the phase-change layer. By assuming that the transition follows a particular functional form with slope determined by a parameter, referred to as the transition length parameter, the slope equation is solved at one specific spatial location only for this parameter. The spatial gradient of the temperature $\partial T/\partial x$ in (1) is determined by the electrical and thermal processes involved during the writing process, and takes into account the geometry, dimensions, and thermal and electrical properties of the system. The term $\partial \sigma_p/\partial T$, on the other hand, describes the temperature dependence of electrical conductivity and is determined by the material properties and the kinetics of the crystallization process. It also describes the relationship between the fraction of crystalline material and the change in electrical conductivity of the phase-change layer. Hence it represents the "hysteresis" characteristics of the phase-change material, as illustrated by the conductivity versus temperature curve shown in Fig. 1.

The specific location at which the slope equation is solved, referred to in this is work as the transition point, is chosen to be the location of the transition temperature isotherm beyond which irreversible transformations in the material take place. This temperature was chosen since it can be determined accurately and reliably from measurements; it represents the location of the peak heat flow in differential thermal analysis[12] or differential scanning calorimetry[13,14] experiments. It can also be determined as the point of optimum slope in resistivity versus temperature measurement curves.[6,15,16] Moreover, this transition temperature is strongly correlated with the kinetics of the crystallization process that may be described by the Johnson–Mehl–Avrami–Kolmogrov (JMAK) equation.[12,13,17]

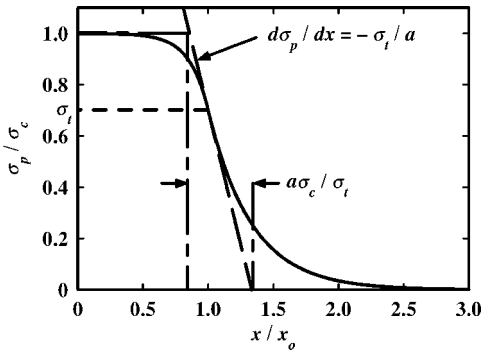

FIG. 2. The assumed exponential conductivity profile in the phase-change layer (continous-line) and its slope (dashed line). Also shown is how the transition length parameter a is related to the extent of the amorphous to crystalline transition region.

The remaining sections of this paper are dedicated to deriving each term of the slope equation in (1) to arrive at an analytical expression for the length of the amorphous to crystalline transition region in phase-change media. Section II introduces the assumed functional form of the amorphous to crystalline transition. This is then used in Sec. III in an electrothermal model involving Joule heating to determine the temperature distribution and gradient in the phase-change layer. Section IV uses the JMAK theory to derive expressions for crystallization rates to be used in the slope theory, and Bruggeman's effective-medium approach to relate the fraction of the transformed crystalline material to the conductivity change in the phase-change layer. These are then combined in the slope equation to arrive at an expression for the amorphous to crystalline transition length in Sec. V where the requirements for small transition lengths, and hence high linear storage densities, are outlined.

To simplify the analyses, it is assumed in the following that the recording layer is thin and hence the temperature and electrical conductivity have no gradients in the vertical direction.

II. TRANSITION PROFILE

A prerequisite for the application of the slope theory is the use of an analytical form for the transition region. In this work, the amorphous to crystalline transition will be assumed to be described by the exponential function (shown in Fig. 2):

$$\sigma_p = \sigma_t \exp[-(x - x_o)/a], \quad x \geqslant x_o, \tag{2a}$$

$$\sigma_p = \sigma_c - (\sigma_c - \sigma_t)\exp\left[\frac{\sigma_t(x - x_o)}{a(\sigma_c - \sigma_t)}\right], \quad x < x_o, \tag{2b}$$

where σ_t is the conductivity of the phase-change material at the transition temperature, which occurs at location x_o, σ_c is the conductivity of the crystalline phase, and a is a parameter that is related to the spatial extent of the amorphous to crystalline transition and will be referred to here as the transition length parameter. In Eq. (2), it is implicit that the conductivity of the amorphous phase is negligible compared to that of the crystalline phase.

The slope of the conductivity profile at the transition position ($x=x_o$) is

$$\left.\frac{\partial \sigma_p}{\partial x}\right|_{x=x_o} = \frac{-\sigma_t}{a}. \tag{3}$$

It can be seen from (3) that the length parameter a determines the slope and hence the extent, $a\sigma_c/\sigma_t$, of the transition region at the transition temperature, as illustrated in Fig. 2.

The choice of the exponential function to describe the spatial distribution of the amorphous to crystalline transition in (2) reflects the large difference in electrical conductivity between the two phases, and the inherent asymmetry of this distribution around the transition temperature. This function also offers the advantage of yielding closed-form solutions to the heat conduction equation, thus maintaining the theory presented here analytical. It is important to note that the choice of the transition distribution does not alter the dependence of the transition length on the fundamental parameters of the system. This was found in magnetic recording where the use of different mathematical functions to represent the symmetrical magnetic transition (including the arctangent, tanh, and error functions) in the magnetic medium affected only slightly the magnitude of the transition length (within 20%) for the different transition functions,[18] but not the dependence on the material properties and head-to-medium interface parameters.

III. TEMPERATURE GRADIENT

It can be shown that the steady-state, thickness-averaged temperature of a thin film of phase-change material in a multilayer structure is given by[19]

$$\frac{\partial^2 T}{\partial x^2} - G(T - T_o) = \frac{-P}{k_p}, \tag{4}$$

where T_o is the ambient temperature (equal to 293 K here), and P is the power per unit volume generated in the phase-change layer due to Joule heating and is defined by $P = \sigma_p|\boldsymbol{E}|^2$ where $\boldsymbol{E}$ is the vector electric field developed in the phase-change layer. The coefficient G includes the thermal properties and thicknesses of the storage medium structure and has units of m^{-2}. Considering as an example the three-layer geometry shown in Fig. 3, the coefficient G is[19]

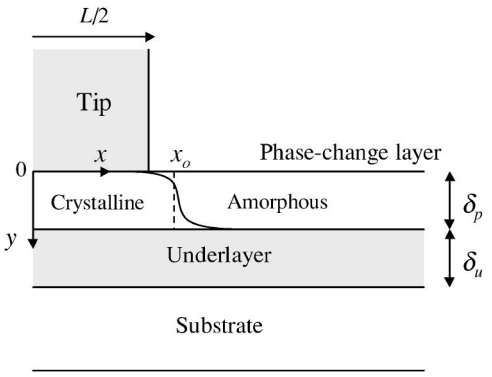

FIG. 3. Geometry of the tip/electrode and material structure used to develop the electrothermal model of the recording system. Symmetry is assumed about the center of the coordinate system which is located at the middle of the tip.

$$G = \frac{1}{k_p \delta_p}\left[H_t + \frac{H_b}{1 + H_b(\delta_u/k_u)}\right], \tag{5}$$

where k_p and k_u are the thermal conductivities of the phase-change layer and underlayer, respectively, δ_p and δ_u are the thicknesses of the phase-change layer and underlayer, respectively, H_b is the thermal-conduction coefficient at the bottom of the underlayer, and H_t is the thermal-conduction coefficient at the top of the phase-change layer. These thermal-conduction coefficients allow the study of the effects of different thermal boundary conditions (insulated when $H \to 0$ and supercooled when $H \to \infty$) and different substrate materials on the temperature distribution in the recording layer.

It is assumed here that the thermal conductivity of the phase-change layer is independent of temperature. This assumption helps us ensure that the solutions are analytical, but is in any case not unreasonable from a physical standpoint. Published experimental measurements of the thermal conductivity of $Ge_2Sb_2Te_5$ showed only a relatively small increase in thermal conductivity from low temperatures up to room temperature (with values 0.24 and 0.53 W/m K at room temperature for the amorphous and crystalline phases, respectively) and indicated phonon-dominated thermal conduction.[20] Above room temperature it might be expected that the electronic contribution could lead to significant further increases in thermal conductivity. However, the electronic contribution in $Ge_2Sb_2Te_5$ forms a relatively small part of the overall thermal conductivity, as can be estimated via the Weidemann–Franz relationship[21] using an activation-type temperature dependence of electrical conductivity.[22,23] Indeed, thermal-conductivity measurements of other amorphous chalcogenides showed little more than a few tens of percent increase in thermal conductivity for temperatures ranging from ambient right up to the crystallization temperature.[24,25] The assumption of a constant thermal conductivity over the temperature ranges of interest in this work is not therefore overly restrictive, and a value of 0.4 W/m K at the transition temperature (lying between the amorphous and crystalline values) is used.

From the symmetry shown in Fig. 3 about the center of the coordinate system, the tip is modeled as a semi-infinite,

infinitely conducting rectangular block having a contact length L with the phase-change layer, and is biased at positive voltage $+V$. The underlayer represents the bottom electrode and is modeled as an infinitely conducting sheet separated from the tip by constant gap u that is equal to the thickness of the phase-change layer (i.e., $u=\delta_p$) and held at ground potential. Considering, for simplicity, only vertical current flow through the phase-change layer, a first-order Padé approximation of the y component of the electric field was found to be[19]

$$E_y(x,y)=\begin{cases} E_o & -L/2 \leqslant x \leqslant L/2 \\ E_o \dfrac{d}{d+2u(|x|-L/2)} & |x|>L/2, \end{cases} \tag{6}$$

where $E_o=V/u$, $d=\pi y(2u-y)$, and y is the distance from the tip to the evaluation point in the phase-change layer with $y<u$. This E_y field represents the source of Joule heating in the phase-change layer.

Having provided the thermal and electrical models of the system, the next step is to determine the required conditions for writing a crystalline mark in an amorphous material. This involves determining the voltage that is required to heat the phase-change layer to the transition temperature and cause irreversible transformation in the material; this will be referred to as the threshold voltage for conduction.[2,3] When G is large and the electrical conductivity in the phase-change layer changes negligibly prior to the creation of an amorphous to crystalline transition, it can be shown that (4) may be approximated well by

$$T-T_o \approx \frac{-P}{k_p G}. \tag{7}$$

Large values of G correspond to the situation where most of the heat generated in the phase-change layer is dissipated vertically through the layer structure, such that the temperature distribution in this layer is determined mainly by the square of the magnitude of the electric-field profile of the tip/electrode arrangement. Setting $T=T_t$ in (7) and solving for the voltage in the region $-L/2 \leqslant x \leqslant L/2$ where the temperature is maximum yield the threshold voltage as

$$V_t = u\sqrt{\frac{k_p G(T_t-T_o)}{\sigma_t}}, \tag{8}$$

where σ_t is the electrical conductivity at the transition location. The location of the transition temperature isotherm at a given voltage may also be determined under these conditions by substituting the electric field in the region $|x|>L/2$ defined in (6) into (7) and solving for x at $T=T_t$. For different ratios of the threshold voltage $F=V/V_t$, where V is the applied voltage, the location of the transition temperature is

$$x_o = \frac{L}{2}+\frac{d}{2u}(F-1), \quad F \geqslant 1, \tag{9}$$

which indicates that at the threshold voltage where $V=V_t$ the transition temperature isotherm is approximately in the close vicinity of the tip corners. The position of the transition temperature isotherm in (9) is used next to determine the temperature gradient in the phase-change layer at the transition temperature.

When an amorphous to crystalline transition has been created, the temperature distribution in the phase-change layer, in the region $|x|>L/2$, is determined by evaluating the power density using the electrical conductivity profile defined in (2a) and the electric field from (6). Substituting this into the heat conduction equation in (4) and solving subject to the boundary conditions that $T=T_t$ at $x=x_o$, and $T=T_o$ as $x\to\infty$ yield the temperature in the phase-change layer as

$$T-T_o = e^{-\sqrt{G}(x-x_o)}[(T_t-T_o)-S(x_o)]+S(x), \quad x>L/2. \tag{10}$$

The particular solution $S(x)$, written in terms of the exponential integral Ei, is given by

$$\begin{aligned} S(x) = \frac{P_o d^2 e^{(x_o-L/2)/a}}{8k_p u^2\sqrt{G}} \Bigg\{ & \alpha e^{\alpha d/2u} e^{\sqrt{G}(x-L/2)} \\ & \times Ei\left(\frac{-\alpha[d+2u(x-L/2)]}{2u}\right) + \beta e^{-\beta d/2u} e^{-\sqrt{G}(x-L/2)} \\ & \times Ei\left(\frac{\beta[d+2u(x-L/2)]}{2u}\right)\Bigg\}, \end{aligned} \tag{11}$$

with $\alpha=\sqrt{G}+1/a$, $\beta=\sqrt{G}-1/a$, and $P_o=\sigma_p E_o^2$.

Differentiating (10) with respect to x and evaluating at $x=x_o$ defined in (9) yield the temperature gradient at the transition position:

$$\begin{aligned} \left.\frac{\partial T}{\partial x}\right|_{x=x_o} = & -\sqrt{G}(T_t-T_o)+\frac{dFG(T_t-T_o)}{2u} \\ & \times\left\{1+\frac{\alpha dF}{2u}e^{\alpha dF/2u}\,\mathrm{Ei}\left(\frac{-\alpha dF}{2u}\right)\right\}. \end{aligned} \tag{12}$$

For values of $\alpha dF/2u>5$, the term in curly brackets on the right-hand side of (12) can be simplified using the approximation $1+\eta e^{\eta}\,\mathrm{Ei}(-\eta)\approx 1/(2+\eta)$, when $\eta>5$ yielding,

$$\left.\frac{\partial T}{\partial x}\right|_{x=x_o} = -\sqrt{G}(T_t-T_o)\left\{\frac{1+a\dfrac{4u}{dF}}{1+a\left(\dfrac{4u}{dF}+\sqrt{G}\right)}\right\}.$$

This can be further simplified by noting that $4ua/dF<1$ leading to the form:

$$\left.\frac{\partial T}{\partial x}\right|_{x=x_o} \approx -\sqrt{G}(T_t-T_o)\left\{\frac{1}{1+a\sqrt{G}}\right\}. \tag{13}$$

Equation (13) represents the value of the temperature gradient at the transition temperature isotherm for applied voltages that are equal to or greater than the threshold value. The absence of voltage terms in (13) indicates that, for this particular structure, the temperature gradient at the transition position has little sensitivity to applied voltages that are greater than the threshold value.

IV. CRYSTALLIZATION KINETICS AND ELECTRICAL CONDUCTIVITY

From the slope equation in (1), the extent of the amorphous to crystalline boundary requires description of the change in the electrical conductivity with temperature. Experimentally, this is represented by conductivity versus temperature measurements such as that shown in Fig. 1. The change in conductivity is associated with the change in crystallization fraction during the transformation process. To include the dependence of electrical conductivity on the crystallization fraction explicitly, the change in conductivity with temperature can be expressed in the form:

$$\frac{\partial \sigma_p}{\partial T} = \frac{\partial \sigma_p}{\partial \chi}\frac{\partial \chi}{\partial T}, \tag{14}$$

where σ_p is the conductivity of the amorphous/crystalline mixture, and χ is the volume fraction of crystalline material in this mixture. Each of these gradients will next be determined at the transition temperature.

A. Crystallization kinetics

The crystallization kinetics of amorphous alloys can be described using the Johnson–Mehl–Avrami–Kolmogorov (JMAK) model where the crystallization fraction as a function of time is given by[26]

$$\chi(t) = 1 - \exp[-(Kt)^n], \tag{15}$$

where n is the Avrami exponent, t is the time, and K is the reaction-rate constant which can be described using the Arrhenius temperature dependence:

$$K = K_o \exp\left(\frac{-E_c}{RT}\right), \tag{16}$$

where E_c is the activation energy, K_o is a frequency factor (which is assumed to be temperature and time independent), T is the absolute temperature, and R is the Boltzmann constant.

To include nonisothermal heating effects during crystallization in the JMAK equation, it would be more convenient to determine the change of crystallization fraction with temperature from the relation:

$$\frac{\partial \chi}{\partial t} = \frac{\partial \chi}{\partial T}\frac{\partial T}{\partial t}, \tag{17}$$

where $\partial\chi/\partial t$ is the crystallization rate and $\partial T/\partial t = \phi$ is the heating rate.

The crystallization rate $\partial\chi/\partial t$ can be determined from the JMAK equation but depends on the functional form of temperature rise with time in the phase-change material. In this work the temperature is assumed, as a first-order approximation, to increase linearly at a constant heating rate ϕ.

$$T = T_o + \phi t, \tag{18}$$

where T_o is the initial temperature and is taken here to be equal to the ambient temperature. Simplified analytical models and more detailed numerical simulations of laser heating in phase-change optical storage disks have indicated that the temperature rise in the phase-change layer involves transient and steady-state stages with a nonconstant heating rate.[27,28] However, at small times after applying the heating source and near the transition or crystallization temperature where interest is focused here, the temperature evolution is almost linear with a constant heating rate[27] and can thus be described by (18) in this region. Moreover, using this linear approximation allows comparison with ramped electrical conductivity versus temperature measurements that are typically used to study and characterize phase-change recording media.

Differentiating the JMAK equation in (15) with respect to time realizing that K is also a function of time yields the crystallization rate:

$$\frac{\partial \chi}{\partial t} = nK^n t^{n-1}\left[1 + \left(\frac{\phi E_c}{RT^2}\right)t\right](1-\chi). \tag{19}$$

Expressing the time t in terms of the crystallization fraction using (15) produces

$$\frac{\partial \chi}{\partial t} = An(1-\chi)\left(K + \frac{\phi E_c}{RT^2}[-\ln(1-\chi)]^{1/n}\right), \tag{20}$$

where $A = [-\ln(1-\chi)]^{(n-1)/n}$.

The two limiting cases of small and high heating rates will be analyzed next since an analytical expression for the crystallization rate at the transition temperature cannot be derived directly from (20). The small heat rate limit corresponds to ramped annealing measurements that are used to characterize phase-change media (for example, resistance measurements,[6,29] and differential scanning calorimetry[14]), while the high heating rate regime simulates the situation of laser recording in optical storage.

1. Small heating rates

For small heating rates and taking that[13] $E_c/RT^2 < 1$, the second term in (20) may be neglected and the rate of change of the crystalline fraction becomes

$$\frac{\partial \chi}{\partial t} = AnK(1-\chi). \tag{21}$$

This reduced form of crystallization rate has the same form as a first-order reaction described by Kissinger.[12] This connection between the modified form of the JMAK and the Kissinger equations implies that, under the small heating rate restriction, the JMAK equation may be used to model nonisothermal reactions.[13,17] It also explains why the use of the Kissinger method for determining the kinetic parameters of crystallization in phase-change media is appropriate in thermal annealing experiments adopted by many workers.[6,15,16,29]

The transition temperature is identified as the temperature of maximum crystallization rate[12] at which $\partial^2\chi/\partial t^2 = 0$. Thus, differentiating (21) with respect to time and assuming that A does not change significantly near the maximum,[13] leads to the following condition at the transition temperature:

$$\frac{\phi E_c}{RT_t^2} = A_t n K_t, \tag{22}$$

where the subscript t denotes the values at the transition temperature with $K_t = K_o e^{-E_c/RT_t}$.

The fraction of crystalline material at the transition temperature, under the small heating rate restriction, may now be found from integration of Eq. (21) and application of condition (22) [the original JMAK equation cannot be used in this case since the above analysis are based on the modified form of the crystallization rate in (21)]. Equation (21) may be integrated exactly and the solution involves the exponential integral. To avoid this, the approximation of Kissinger for a first-order reaction[12] can be used and the fraction of crystallized material becomes

$$-\ln(1-\chi) = \frac{AnRT^2}{\phi E_c} K_o \exp\left(\frac{-E_c}{RT}\right)\left(1-\frac{2RT}{E_c}\right). \tag{23}$$

Substituting (22) into (23) at the transition temperature yields

$$-\ln(1-\chi_t) = 1 - \frac{2RT_t}{E_c} \approx 1, \tag{24}$$

and the crystallization fraction at the transition temperature χ_t is approximately equal to

$$\chi_t \approx 1 - 1/e = 0.6321\cdots. \tag{25}$$

Equation (24) also implies that $A_t \approx 1$.

The crystallization rate at the transition temperature can now be determined by substituting the condition (22) and the crystalline fraction in (25) into (21),

$$\left.\frac{\partial \chi}{\partial t}\right|_{T_t} = \frac{\phi E_c}{eRT_t^2}. \tag{26}$$

The change in the crystalline fraction with temperature, at the transition temperature, simply follows for the linear temperature rise and small heating rate as

$$\left.\frac{\partial \chi}{\partial T}\right|_{T_t} = \frac{E_c}{eRT_t^2}. \tag{27}$$

The influence of the heating rate on the crystallization fraction enters implicitly in (27) through the transition temperature T_t, and this dependence is clarified in the Appendix.

2. High heating rates

This limit approximates, for electrical probe recording, the case of an applied voltage step with a very short rise time. It can also represent the case of isothermal heating experiments on phase-change media. In this case, the second term in (20) dominates and the crystallization rate becomes

$$\frac{\partial \chi}{\partial t} = \frac{-\phi n E_c}{RT^2}(1-\chi)\ln(1-\chi). \tag{28}$$

At the maximum crystallization rate, the following condition must be satisfied:

$$-\ln(1-\chi_t) = 1 - \frac{2RT_t}{nE_c} \approx 1. \tag{29}$$

This indicates that the fraction of the crystalline material at the transition temperature at very high heating rates is also approximately equal to 0.63, as in (25). Substituting this condition in (28) yields the crystallization rate at the transition temperature as

$$\left.\frac{\partial \chi}{\partial t}\right|_{T_t} = \frac{\phi n E_c}{eRT_t^2}. \tag{30}$$

The gradient of the fraction of the crystalline material transformed with temperature is therefore, using (18), given by

$$\left.\frac{\partial \chi}{\partial T}\right|_{T_t} = \frac{nE_c}{eRT_t^2}, \tag{31}$$

which has the same functional form and dependence as Eq. (27) for small heating rates, except that the gradient of the transformation with temperature at high heating rates is increased by a factor of n. Equation (31) can be used to represent an upper limit for this gradient and, as will be shown later, a lower limit for the transition length.

B. Electrical conductivity of phase-change material

The fraction of the crystalline material transformed as a function of temperature $\partial\chi/dT$ was determined in the preceding section. The change in the crystalline fraction with temperature is also accompanied by a change in the electrical conductivity of the material. It is the change of conductivity of the phase-change material with temperature $\partial\sigma_p/\partial T$ that is required to be found to solve the slope equation in (1) for the transition length. $\partial\sigma_p/\partial T$ can be determined using (14) where the term $\partial\sigma_p/\partial\chi$ links the change in conductivity with crystalline fraction and will be determined next.

According to Bruggeman's symmetrical effective-medium theory,[30] the conductivity σ_p of a mixture of two types of spherical inclusions, in this work crystalline material with fraction χ and an amorphous material with fraction $(1-\chi)$, is given by

$$\chi\frac{\sigma_c - \sigma_p}{\sigma_c + (m-1)\sigma_p} + (1-\chi)\frac{\sigma_a - \sigma_p}{\sigma_a + (m-1)\sigma_p} = 0, \tag{32}$$

where σ_c and σ_a are the electrical conductivities of the crystalline and amorphous phases, respectively, and $m=1$, 2, or 3 representing the dimensionality of the system. This theory predicts a critical volume fraction or percolation threshold, χ_c, for the formation of filaments or conducting pathways of the crystalline material for a three-dimensional system at $\chi_c = 1/3$. Numerical computations have shown, however, that in a mixture of conducting and nonconducting materials, only about 0.15–0.17 fraction of the conducting material is needed to create continuous conducting pathways.[30] Amongst the many reasons for this discrepancy, is the one based on the fact that spherical inclusions provide the least surface area and must obviously occupy a more appreciable fraction of the total volume before guaranteeing enough contact for the existence of conducting filaments. Thus, nonspherical inclusions (for example, ellipsoids) were suggested

to provide contact more easily than spheres with the same volume and thus achieving lower percolation thresholds.[30,31] By including the effects of coupling between the conducting inclusions in the form of clusters or chains in Eq. (32), it was shown that it is possible to obtain a percolation threshold of 0.156 that is close to the expected value from numerical calculations.[32] Generally in these theories, changing the percolation threshold involves changing the coefficient of σ_p in the denominator of (32).

Based on these theories and observation made by other workers, the effective-medium theory approach was generalized for any percolation threshold and extended to model different material behaviors in a phenomenological approach by McLachlan *et al.*[33] This involved rewriting Bruggeman's formula for a mixture of two inclusions in the form:

$$\chi\frac{\sigma_c^{1/r}-\sigma_p^{1/r}}{\sigma_c^{1/r}+D\sigma_p^{1/r}}+(1-\chi)\frac{\sigma_a^{1/s}-\sigma_p^{1/s}}{\sigma_a^{1/s}+D\sigma_p^{1/s}}=0, \tag{33}$$

where r and s are exponents that control the extent of the change in conductivity with crystallization fraction, and $D=(1-\chi_c)/\chi_c$. When $r=s=1$ and $\chi_c=1/3$, Bruggeman's equation for a three-dimensional system is obtained. The form of Eq. (33) is very useful to investigate the effect of different values of the percolation threshold on the transition length, and also to model cases where the observed electrical conductivity "leads" the fraction of the crystallized material in conductivity measurements during amorphous to crystalline transformation[34] in a unified manner.

When the electrical conductivity of the crystalline material is much larger than that of the amorphous material (i.e., $\sigma_c > \sigma_a$), Eq. (33) can be solved for the conductivity of the mixture and reduces to

$$\sigma_p=\sigma_c\left(\frac{\chi-\chi_c}{1-\chi_c}\right)^r, \quad \chi_c \leqslant \chi \leqslant 1. \tag{34}$$

Differentiating (34) with respect to χ and evaluating at the transition temperature yields the change in electrical conductivity with crystalline fraction as

$$\left.\frac{\partial\sigma_p}{\partial\chi}\right|_{T=T_t}=\frac{r\sigma_t}{\chi_t-\chi_c}, \tag{35}$$

where σ_t is the conductivity of the phase-change layer at the transition temperature and can be determined from (34) when the fraction of the crystalline material at this temperature is known.

The change in conductivity with temperature including the dependence on crystallization fraction can now be derived, for the small heating rate case, by substituting (27) and (35) into (14) to yield

$$\left.\frac{\partial\sigma_p}{\partial T}\right|_{T=T_t}=\frac{\sigma_t r}{(\chi_t-\chi_c)}\frac{E_c}{eRT_t^2}. \tag{36}$$

The high heating rate case is given simply by multiplying the right-hand side of Eq. (36) by n.

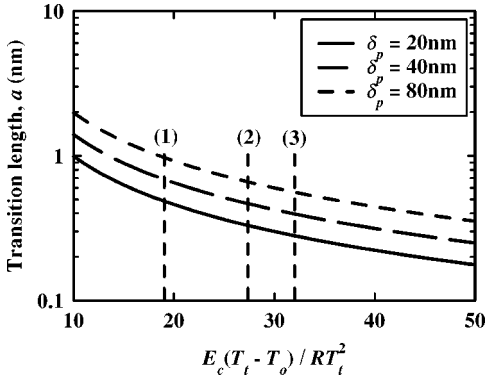

FIG. 4. Transition length as a function of the dimensionless ratio $E_c(T_t-T_o)/RT_t^2$ for different phase-change layer thicknesses. The parameters for the calculations are $\delta_u=20$ nm, $L=20$ nm, $u=\delta_p$, $y=\delta_p/2$, $k_p=0.4$ W/m K, $k_u=50$ W/m K, $H_t=0$ W/m^2 K, $H_b=2\times10^8$ W/m^2 K, $\chi_c=0.15$, and $r=1$. The indicated numbers refer to the following phase-change materials: (1) $Ge_2Sb_2Te_5$, (2) AglnSbTe, and (3) $Ge_4Sb_1Te_5$.

V. TRANSITION LENGTH

The extent of the amorphous to crystalline transition along the phase-change layer can now be estimated using the slope-theory approach. This is achieved by substituting into (1) the spatial slope of the electrical conductivity from (3), the spatial gradient of the temperature in (13), and the change of electrical conductivity with temperature described in (36), all evaluated at the transition temperature. Solving for the transition length parameter a yields

$$a=\frac{1/\sqrt{G}}{\left(\frac{r(T_t-T_o)}{\chi_t-\chi_c}\right)\left(\frac{E_c}{eRT_t^2}\right)-1}. \tag{37}$$

Equation (37) outlines the requirements for short transition lengths and therefore the shortest possible distance between two adjacent bits. The first requirement is a small thermal characteristic length $1/\sqrt{G}$; this allows the temperature distribution in the phase-change layer to follow the electric field and increases the temperature gradient at the transition temperature isotherm. This happens when the heat generated in the phase-change layer dissipates vertically through the sandwiching layers rather than laterally along the phase-change layer itself. A small thermal characteristic length also demands a thin recording layer as indicated in Eq. (5). The other requirement for small transition lengths is to maximize the ratio of activation energy to transition temperature E_c/T_t. This increases the crystallization rate leading to a sharper slope of the conductivity versus temperature characteristic at the transition temperature. Increasing the heating rate also reduces the transition length by multiplying the ratio of activation energy to transition temperature by the Avrami exponent n.

Figure 4 illustrates the calculated transition length using (37) for the structure shown in Fig. 3, as a function of the dimensionless quantity $E_c(T_t-T_o)/RT_t^2$ for different thicknesses of the phase-change layer. This figure illustrates the above requirements for small transition lengths. Also highlighted in this figure are the transition lengths for three different values of the ratio E_c/T_t corresponding to three phase-

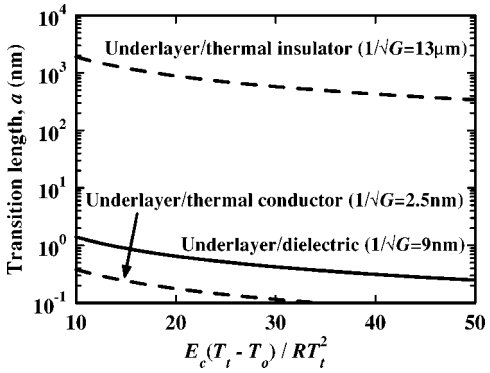

FIG. 5. Calculated transition lengths for different thermal boundary conditions between the underlayer and substrate, simulating different substrate materials. For underlayer/dielectric $H_b = 2\times10^8$ W/m^2 K, for underlayer/thermal conductor $H_b \to \infty$, and for underlayer/thermal insulator $H_b \to 0$. Also shown are the calculated thermal characteristic lengths $1/\sqrt{G}$ for each boundary. The calculation parameters are the same as in Fig. 4 and using $\delta_p = 40$ nm.

change materials typically used in data storage applications: (1) $Ge_2Sb_2Te_5$ with $E_c = 2.24 \pm 0.11$ eV (Ref. 6) and $T_t = 428$ K;[14] (2) AglnSbTe with $E_c = 3.03 \pm 0.17$ eV (Ref. 16) and $T_t = 453$ K;[14] and (3) $Ge_4Sb_1Te_5$ with $E_c = 3.48 \pm 0.12$ eV (Ref. 15) and $T_t = 463$ K.[14] The values quoted for the transition temperatures were obtained from differential scanning calorimetry[14] at a heating rate of 5 K/min. It can be seen from the figure that the material with the highest E_c/T_t ratio, $Ge_4Sb_1Te_5$, is predicted by the slope-theory approach to produce the smallest transition length.

Figure 5 illustrates the effect of different thermal boundary conditions, included in the thermal length $1/\sqrt{G}$, on the transition length. A high thermal-conductivity substrate provides a heat sink for the heat flux generated in the phase-change layer and makes the temperature distribution follow closely the tip electric field (short thermal length). This increases the temperature gradient at the transition location, thus reducing the transition length. A thermally insulated substrate, on the other hand, forces the temperature distribution in the phase-change layer to spread laterally, thus reducing the temperature gradient at the transition location and increasing the transition length.

For a 20-nm-thick phase-change layer, for example, a transition length parameter of $a = 0.48$ nm is predicted for $Ge_2Sb_2Te_5$ using the structure shown in Fig. 3. This corresponds to a transition region $a\sigma_c/\sigma_t$ around 4.8 nm ($\sigma_c/\sigma_t \approx 10$ from Ref. 6). Applying a series of "on" and "off" voltages to the phase-change layer (representing the binary states 1 and 0) when the tip is moving in continuous contact with the material produces a sequence of amorphous to crystalline transitions. A reasonable estimate for the maximum achievable linear density in this case might be obtained by assuming that transition centers are separated by $2a\sigma_c/\sigma_t$, thus avoiding excessive overlap between neighboring transitions. This would yield a linear storage density of around 2600×10^3 phase transitions per inch of the medium.

VI. SUMMARY

A theoretical approach to predicting the linear density in contact electrical probe recording on phase-change media has been developed. This approach, inspired by the slope theory used in magnetic recording, combined the electrothermal factors and the material properties in a self-consistent approach to predict the extent of an amorphous to crystalline transition. This theory showed that smaller transition lengths can be obtained when heat produced in the phase-change layer due to Joule heating is made to flow vertically through the adjacent layers such as to reduce the thermal wavelength in the phase-change layer. Moreover, a material with higher activation energy to transition temperature ratio and high heating rates is needed to reduce the transition length.

APPENDIX

At small heating rates, the condition in (22) at the peak crystallization rate can be rewritten as

$$\frac{\phi}{T_t^2} = \Gamma \exp\left(\frac{-E_c}{RT_t}\right), \tag{A1}$$

where $\Gamma = A_t R n K_o / E_c$ is a constant. Taking the natural logarithm of the above yields the Kissinger formula[12] describing a straight-line relationship between the heating rate and reciprocal of the transition temperature whose slope is E_c/R:

$$\ln\left(\frac{\phi}{T_t^2}\right) = \ln\Gamma - \left(\frac{E_c}{RT_t}\right). \tag{A2}$$

Solving (A2) for the transition temperature yields

$$T_t = \frac{E_c}{2RW(z)}, \tag{A3}$$

where $W(z)$ is the Lambert W function and z is defined by

$$z = \frac{1}{2}\sqrt{\frac{nA_tE_cK_o}{\phi R}}. \tag{A4}$$

The explicit dependence of the transition temperature on heating rate is clearly shown in (A3) and (A4).

Determination of the Lambert W function in (A3) requires the evaluation of an infinite series. Fortunately since z in (A4) is normally large, an asymptotic expansion of the W function accurate for $z \geqslant 3$ exists; the first three terms of this expansion provide sufficient accuracy and are given by

$$W(z) \cong \ln(z) - \ln[\ln(z)] + \frac{\ln[\ln(z)]}{\ln(z)}, \quad z \geqslant 3. \tag{A5}$$

Figure 6 compares the measured transition temperatures for an 80-nm $Ge_2Sb_2Te_5$ film using nonisothermal four-point-probe resistance measurements,[6] with the calculated values using (A3) at different heating rates. The transition temperatures in these experiments were determined from the minimum in the resistivity versus temperature curves. The thermodynamic and kinetic parameters used in calculating the transition temperatures were obtained, for the same material, from isothermal measurements[35] and are provided in the figure caption. The good agreement between the measured and calculated values illustrates the potential of using the JMAK equation, subject to the small heating rate restriction, to describing nonisothermal reactions. At high heating rates, the theoretical transition temperature values in Fig. 6 begin to deviate from the measured ones, as expected.

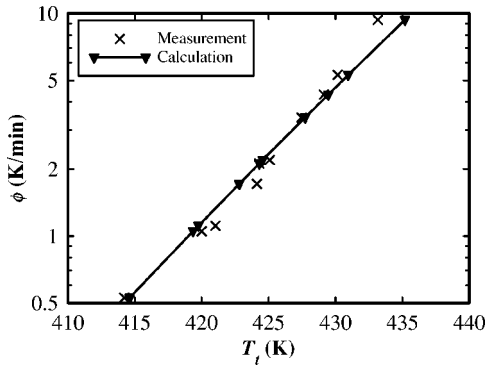

FIG. 6. Measured transition temperatures as functions of the heating rate for $Ge_2Sb_2Te_5$ obtained from four-point-probe resistivity measurements in Ref. 6, compared with the calculated values from Eq. (A3). The parameters used for the calculations were obtained from isothermal optical reflectivity measurements in Ref. 35 and are $E_c=2.1$ eV, $K_o=1.5\times10^{22}$ s^{-1}, and $n=2.5$. It was also assumed that $A_t=1$.

In the high heating rate regime (or equivalently isothermal annealing) the condition $K_t t\approx 1$ is arrived at by comparing (29) with the JMAK equation in (15) at the transition temperature. Substituting for K_t from (16), an expression for the transition temperature can be derived exactly and is given by

$$T_t = \frac{E_c}{R\ln(K_o t)}, \tag{A6}$$

showing the explicit dependence of the transition temperature on heating time t in this case.

[1]H. Kado and T. Tohda, Jpn. J. Appl. Phys., Part 1 **36**, 523 (1997).
[2]T. Gotoh, K. Sugawara, and K. Tanaka, J. Non-Cryst. Solids **299–302**, 968 (2002).
[3]T. Gotoh, K. Sugawara, and K. Tanaka, Jpn. J. Appl. Phys., Part 2 **43**, L818 (2004).
[4]D. Saluel, J. Daval, B. Bechevet, C. Germain, and B. Valon, J. Magn. Magn. Mater. **193**, 488 (1999).
[5]K. Sugawara, T. Gotoh, and K. Tanaka, Jpn. J. Appl. Phys., Part 2 **43**, L676 (2004).
[6]I. Friedrich, V. Weidenhof, W. Njoroge, P. Franz, and M. Wuttig, J. Appl. Phys. **87**, 4130 (2000).
[7]M. Armand, C. D. Wright, M. M. Aziz, and S. Senkader, *Optical Data Storage 2003*, SPIE Vols. 5069 and 150, edited by M. O'Neill and N. Miyagawa (SPIE, Bellingham, WA, 2003).
[8]C. D. Wright, M. M. Aziz, M. Armand, S. Senkader, and W. Yu, Mater. Res. Soc. Symp. Proc. **803**, 61 (2003).
[9]M. L. Williams and R. L. Comstock, in *An Analytical Model of the Write Process in Digital Magnetic Recording*, edited by C. D. Graham, Jr. and J. J. Rhyne, AIP Conf. Proc. No. 5 (AIP, New York, 1971), p. 738.
[10]V. J. Maller and B. K. Middleton, Radio Electron. Eng. **44**, 281 (1974).
[11]J. J. Miles, D. McKirdy, R. W. Chantrell, and R. Wood, IEEE Trans. Magn. **39**, 1876 (2003).
[12]H. E. Kissinger, Anal. Chem. **29**, 1702 (1957).
[13]A. A. Abu-Sehly, Physica B **325**, 372 (2003).
[14]J. Kalb, E. Spaepen, and M. Wuttig, J. Appl. Phys. **93**, 2389 (2003).
[15]D. Wamwangi, W. Njoroge, and M. Wuttig, Thin Solid Films **408**, 310 (2002).
[16]W. K. Njoroge and M. Wuttig, J. Appl. Phys. **90**, 3816 (2001).
[17]D. W. Henderson, J. Non-Cryst. Solids **30**, 301 (1979).
[18]M. M. Aziz, Ph.D. thesis, University of Manchester, 1999.
[19]M. M. Aziz and C. D. Wright, J. Appl. Phys. (unpublished).
[20]E. Kim, S. Kwun, S. Lee, H. Seo, and J. Yoon, Appl. Phys. Lett. **76**, 3864 (2000).
[21]J. R. Drabble and H. J. Goldsmid, *Thermal Conduction in Semiconductors* (Pergamon, New York, 1961).
[22]K. Nakayama, K. Kojima, F. Hayakawa, Y. Imai, A. Kitagawa, and M. Suzuki, Jpn. J. Appl. Phys., Part 1 **39**, 6157 (2000).
[23]K. Morales-Sanchez, E. F. Prokhorov, A. Mendoza-Galvan, and J. Gonzalez-Hernandez, Vacuum **69**, 361 (2003).
[24]K. I. Amirkhanov, Y. B. Magomedov, and S. M. Ismailov, Sov. Phys. Solid State **17**, 2359 (1976).
[25]K. I. Amirkhanov, Y. B. Magomedov, S. M. Ismailov, and K. O. Alieva, Sov. Phys. Semicond. **13**, 349 (1979).
[26]M. C. Weinberg, D. P. Birnie, and V. A. Shneidman, J. Non-Cryst. Solids **219**, 89 (1997).
[27]C. A. Volkert and M. Wuttig, J. Appl. Phys. **86**, 1808 (1999).
[28]D. Kim, S. J. Kim, S. H. An, and S. Y. Kim, Jpn. J. Appl. Phys., Part 1 **42**, 5107 (2003).
[29]E. Morales-Sanchez, E. F. Prokhorov, J. Gonzalez-Hernandez, and A. Mendoza-Galvan, Thin Solid Films **471**, 243 (2005).
[30]R. Landauer, AIP Conf. Proc. **40**, 2 (1978).
[31]S. Norrman, T. Andersson, C. G. Granqvist, and O. Hunderi, Phys. Rev. B **18**, 674 (1978).
[32]C. G. Granqvist and O. Hunderi, Phys. Rev. B **18**, 1554 (1978).
[33]D. S. McLachlan, K. Cai, and G. Sauti, Int. J. Refract. Met. Hard Mater. **19**, 437 (2001).
[34]D. Kim, F. Merget, M. Laurenzis, P. Haring-Bolivar, and H. Kurz, J. Appl. Phys. **97**, 083538 (2005).
[35]V. Weidenhof, I. Friedrich, S. Ziegler, and M. Wuttig, J. Appl. Phys. **89**, 3168 (2001).